



Rapid and sensitive ethanol sensor based on hollow Au/V₂O₅ nanotubes via emulsion-electrospinning route



Wen Zeng^{a,b,*}, Weigen Chen^b, Zhenyu Li^{b,c,d,*}, He Zhang^a, Tianming Li^a

^a College of Materials Science and Engineering, Chongqing University, Chongqing 400044, PR China

^b State Key Laboratory of Power Transmission Equipment & System Security and New Technology, Chongqing University, Chongqing 400044, PR China

^c Alan G. MacDiarmid Institute, Jilin University, Changchun 130012, PR China

^d Institute for Frontier materials, Deakin University, Geelong, Victoria 3216, Australia

ARTICLE INFO

Article history:

Received 13 August 2014

Received in revised form 19 January 2015

Accepted 25 January 2015

Available online 28 January 2015

Keywords:

A. Oxide

B. Chemical synthesis

B. Crystal growth

A. Nanostructures

D. Electrical properties

ABSTRACT

Hollow electrospun V₂O₅ and Au/V₂O₅ nanotubes have been successfully synthesized by combining emulsion electrospinning (EE) and post calcination treatment. Immiscible polyvinyl pyrrolidone (PVP)/metal salts/dimethylformamide (DMF) solution and polystyrene (PS)/DMF solution are chosen for the EE to form PS@(PVP/metal salts) core-sheath nanofibers, in which PS nanorods were formed and encapsulated within in the PVP/metal salts nanofibers owing to the stretching forces and de-emulsified force during the electrospinning. Excellent sensitivity and rapid response–recovery behaviors against ethanol have been successfully achieved based on our hollow ceramic (V₂O₅ and Au/V₂O₅) nanotubes.

© 2015 Elsevier Ltd. All rights reserved.

1. Introduction

Prompted by the increasing concerns on health and safety issues arising from air pollution, the monitor of inflammable, explosive, and toxic gaseous target molecules within the environment in time has attracted tremendous effort [1–5]. Among all the gas sensors investigated, semiconducting metal oxides (SMO) gas sensors have gained special focus in fundamental science and practice owing to their high sensitivity, low cost, simple fabrication, and good compatibility with microelectronic processes [6–9]. In general, the sensing mechanism of SMO gas sensors is based on the variation of conductance induced by the interaction between the target gas molecules and the adsorbed oxygen species on the surface of SMO [10]. Thus, nanoscale SMO is of current interest owing to their high surface–volume ratio, increased surface activity and strong adsorption of target gas molecules. These effects can enable the fast adsorption/desorption, and diffusion of target gas molecules on their surface and result in enhanced gas sensing behaviors (high sensitivity, fast response/recovery, low detection limitation) [11–15].

Among all the conventional metal oxides, vanadium pentoxide (V₂O₅) has attracted considerable interest over decades driven by its intrinsic multiple valency, wide optical band gap, good chemical/thermal/thermoelectric performances, etc. [16–30]. Recently, many efforts have been put in the investigation of V₂O₅-based gas sensors. For example, Liu et al. fabricated V₂O₅ nanobelts and investigated their ethanol sensing performances [31]. Dhayal Raj et al. explored the ethanol and ammonia sensing performances based on V₂O₅ nanorods [32]. Modafferi et al. investigated the ammonia sensing performances of electrospun V₂O₅ fibers [33]. However, more or less, these sensors have a limited maximum response, high optimal operating temperature, and insensitive selectivity, which still need to be further improved. Naturally, it is believed that increase the surface area and introduce active agent can effectively improve the sensing performance [34].

As a valid spillover inducer and catalyst, Au introduced in the V₂O₅ may provide more active sites and facilitate electron transfer [35]. Herein, we report the development of rapid and sensitive ethanol gas sensor based on hollow V₂O₅ and Au/V₂O₅ electrospun nanotubes. Such hollow electrospun nanotubes were obtained by combining emulsion electrospinning (EE) and post calcination treatment. The ethanol sensing performances of the as-prepared hollow V₂O₅ and Au/V₂O₅ electrospun nanotubes have been investigated. The results revealed that the as-prepared samples exhibited good sensitivity to ethanol with rapid response/recovery behaviors.

* Corresponding author at: College of Materials Science and Engineering, Chongqing University, Chongqing 400044, PR China. Tel.: +86 13658376869.
E-mail address: wenzeng@cqu.edu.cn (W. Zeng).

2. Experiment

2.1. Chemical

N,N-Dimethyl formamide (DMF: >99%), vanadyl acetylacetonate ($\text{VO}(\text{acac})_2$), gold(III) chloride trihydrate ($\text{HAuCl}_4 \cdot 3\text{H}_2\text{O}$), and polyvinyl pyrrolidone (PVP, $M_w = 1,300,000$) were purchased from Aldrich. Polystyrene with an average molecular weight of 100,000 g/mol was obtained from BDH Chemicals Ltd. All chemicals were used as received without any further purification.

2.2. Preparation of immiscible PVP/metal salts/DMF@PS solution

In a typical procedure, immiscible solution was formed by mixing PVP/metal salts/DMF solution and PS/DMF solution.

For PVP/metal salts/DMF solution: 1.2 g of $\text{VO}(\text{acac})_2 + 0.09$ g of $\text{HAuCl}_4 \cdot 3\text{H}_2\text{O}$ (the molar ratio of V:Au is 100:5) were dissolved into 18 mL of DMF under vigorous stirring for 2 h. Subsequently, 2.7 g of PVP were added into the above solution under vigorous stirring for 6 h.

For PS/DMF solution: 3.2 g of PS was dissolved into 16 mL of DMF under vigorous stirring for 12 h by fixing the temperature at 90 °C. Then the solution was cooled down to room temperature. Finally, those two solutions were mixed together under vigorous stirring for 12 h at room temperature.

For comparison, solutions without containing element Au were also prepared using the same procedure.

2.3. Electrospinning

Precursor nanofibers were prepared using a conventional electrospinning setup [36]. A high DC voltage (20 kV) was provided between the tip of needle and the collector (Al foil) at a distance of 20 cm. The flow rate is fixed at 2 mL/h. Finally, the fiber membrane were peeled off from the collector and transferred onto ceramic boat.

2.4. Post calcination treatment

The calcination was performed in air to remove the organic constituents of PVP/PS and crystallize the V_2O_5 or $\text{Au}/\text{V}_2\text{O}_5$ nanotubes. The whole calcination was divided into following steps. Step i: heat the precursors from room temperature to 330 °C with the heating rate of 5 °C/min and last for 2 h. Step ii: heat the sample from 330 °C to 430 °C with the heating rate of 2 °C/min and last for 30 min then cool down to room temperature.

2.5. Characterization of crystalline structures and morphologies

The optical images of the emulsion solution of PVP and PS were obtained using an optical microscope. The morphologies and structures of the samples before and after post calcination treatment were investigated by the scanning electron microscope (SEM Supra 55VP). Crystal structures were measured by X-ray diffraction (XRD, Scintag XDS 2000 diffractometer with a $\text{Cu K}\alpha$ radiation, $\lambda = 1.5046 \text{ \AA}$).

2.6. Fabrication of the sensing devices

The nanofibers were mixed with deionized water at a fiber/water ratio of 100:15 (wt/wt), and the mixture was ground into a paste, which was spin-coated onto a ceramic tube with a pair of pre-printed gold electrodes. A Pt heating wire was inserted into the tube to form a side-heated gas sensor. The sensor device was dried for 2 days at room temperature. Prior to gas sensing measurement, the entire devices (nanofibers with ceramic tube) were aged at 300 °C for 12 h. During the measurement, all the devices were stabilized at each testing temperature for at least 6 h.

2.7. Characterization of sensing performances

Sensing properties were measured using a static flow system, CGS-8 intelligent test system (Beijing Elite Tech Co., Ltd., China), which composed a heater, a gas distributor and a data acquisition system. Resistance change was recorded during exposing the sensor device to ethanol-containing air, using the CGS-8 intelligent test system. When the response reached a constant value, the device was then recovered by exposing to pure air. The gas sensor response (R_a/R_g) was defined as the ratio of device resistance in air (R_a) and in testing gas (R_g) at the same temperature [37]. The test was performed in a temperature range of 100 °C–300 °C. Certain amount of ethanol liquid was measured by a needle and then evaporated into well-defined concentration of ethanol gas in the reaction chamber. The response time was defined as the time taken by the sensor device to achieve 90% change of the resistance during exposure in the test gas, while the recovery time was defined as the time required for recovery of 90% resistance in pure air [38].

3. Results and discussion

In our experiment, emulsion electrospinning [39–42] has been used for the fabrication of hollow nanostructures. In general, PS drops would turn into rods driven by stretching forces and de-emulsified force during the electrospinning and subsequently act

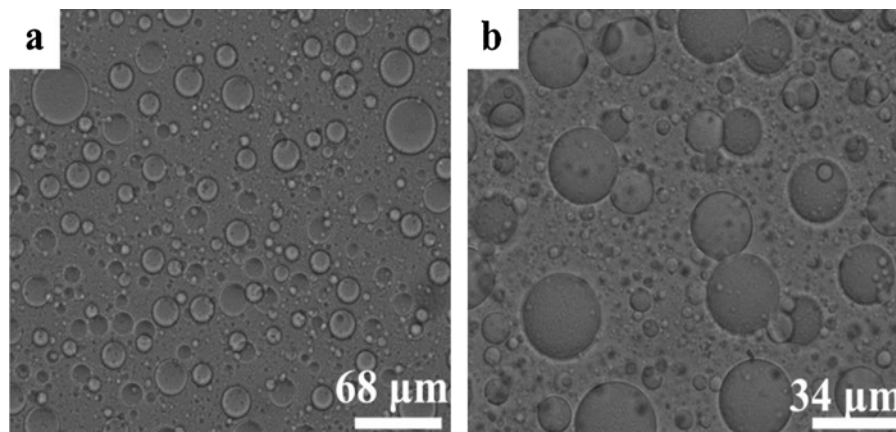


Fig. 1. Optical microscope images of the PS immiscible drops in PVP/metal salt/DMF solution.

as templates in the formation of nanotubes during post calcination treatment. It is of important significance to confirm the presence of PS drops, so the characterization of phase separation within the solution has been carried out by optical microscope. Fig. 1 shows the typical optical images of the solution with low and high magnifications, respectively, indicating PS micro/nano-scaled drops dispersed within the PVP/metal salt solution. During the electrospinning, those PS drops were stretched into elliptical shape within the fiber to form a metal salt poor zone. Meanwhile, PVP/metal salt layer was formed on the surface of the whole fiber. After calcination, hollow metal oxide nanotubes were obtained.

Fig. 2 shows the XRD patterns of Au-modified and bare V_2O_5 nanotubes. For pure V_2O_5 nanotubes (Fig. 2a), the diffraction pattern shows a typical orthorhombic V_2O_5 structure (JCPDS No. 41-1426), which is also presented in the pattern of Au/ V_2O_5 . Moreover, the obviously new diffraction peaks (Fig. 2b), corresponding to the Au (111) and (200), confirm the presence of face-centered cubic (fcc) Au (JCPDS No. 65-2870). It is evident that the decoration of Au nanoparticles does not change the crystallite structure of V_2O_5 nanotubes. A further EDS analysis of the products, shown in Fig. 3, indicates that the Au/ V_2O_5 nanocomposites are composed of three elements: V, Au and O. Combined with the result of XRD, one can conclude that Au element was successfully introduced.

To clearly track such change, the morphologies of the precursors and the final hollow structures have been characterized by SEM as shown Fig. 4. Fig. 4a and b shows the PVP/PS/VO(acac)₂ precursor nanofiber with low and high magnifications, respectively. The diameter of the precursor is ca. 800 nm, and the surface is very smooth. The addition of golden salt does not change the morphologies of the precursors but decreases in diameter to ca. 500 nm, as shown in Fig. 4c and d. After the calcination, both the two nanostructures are formed into nanotubes with the same average diameter of ca. 220 nm, indicating more serious shrinkage of bare V_2O_5 during the calcination, which leads to bigger hole size as obviously shown in Fig. 4e–h. Comparing with V_2O_5 nanostructures, some nanoparticles (white dots, average diameter: 20 ± 5 nm, see the area circled in Fig. 4h) throughout the Au/ V_2O_5 nanocomposites, indicating the existence of Au nanoparticles. Conclusively, except normal removal of organic reagents and corresponding shrinkage after high-heat treatments, the two samples still keep fiber-like structures, indicating their structural stability.

It is well known that the optimal operating temperature is a key factor within the gas sensing performances, which can be obtained by performing the gas sensing measurement at different temperatures. Fig. 5a presents the response to 100 ppm of ethanol of V_2O_5 and Au/ V_2O_5 nanotubes. Both samples exhibited volcano-shape curves, confirming that the optimal operating temperature of V_2O_5 and Au/ V_2O_5 nanotubes is 200 °C and 220 °C, respectively. Au/ V_2O_5 nanotubes exhibited enhanced response in contrast to

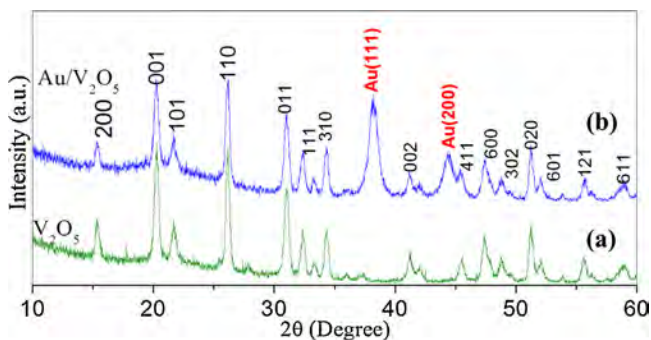


Fig. 2. The XRD patterns of (a) V_2O_5 and (b) Au/ V_2O_5 nanotubes.

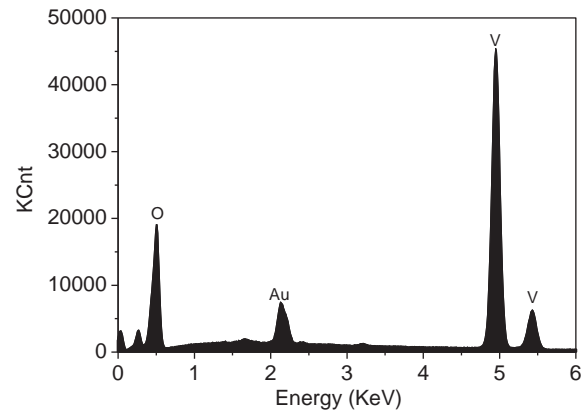
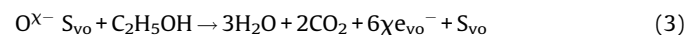
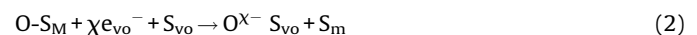


Fig. 3. EDS of Au/ V_2O_5 nanotubes.

pure V_2O_5 . Fig. 5b presents the response/recovery behaviors of V_2O_5 and Au/ V_2O_5 nanotubes against 100 ppm ethanol at their respectively optimal operating temperature. The response/recovery time of pure V_2O_5 is 5 s/5 s and the sensing response (Ra/Rg) is ~ 2.6 . As for the Au/ V_2O_5 nanotubes, enhanced sensing response (~ 2.7) and slightly prolonged response/recovery behavior (7 s/5 s).

The dynamic ethanol sensing transients of two sensors at different concentrations, ranging from 200 to 500 ppm, are shown in Fig. 6. It is obvious that the responses of the both two sensors increase with the ethanol gas concentration increasing, and under each certain concentration (200, 300, 400, 500 ppm in this work), the Au/ V_2O_5 based sensor shows higher sensitivity than that of the bare one. On the other hand, there seem to be no significant differences in response–recovery times of the two sensing materials toward each of the same ethanol gas concentration, which indicates that Au modifying probably has slight influence on dynamics performance of V_2O_5 , for the positive function of Au is counteracted by lower porosity somewhat. Nevertheless, the excellent response–recovery performances of the two sensing materials make them promising candidates as sensors in practical use. As an initial step, we had selected this mass ratio deliberately and had not addressed the dependence of gas-sensing properties on the mass ratio, which remains as a future task.

The simulated morphologies and sensing mechanism of bare V_2O_5 nanotubes and Au/ V_2O_5 nanotubes were presented in Fig. 7. In general, when the Au/ V_2O_5 based sensor is exposed to air, the electrons on the V_2O_5 surface transfer to the Au nanoparticles due to the Schottky contacts between the Au and V_2O_5 nanoparticles [43]. At the same time, the introduced Au nanoparticles have a spill-over effect which consists in catalytic activation of oxygen dissociation, promote the molecule–ion conversion level and dissociate oxygen into oxygen species O^{X-} (O_2^- , O^- and O^{2-}), which then transport and distribute onto both the outer and inner surface of the nanotubes [35]. After ethanol gas in, due to the catalytic effect, Au nanoparticles can facilitate the sensing reaction between the surface O^{X-} and ethanol molecules, releasing the trapped electrons back to V_2O_5 [44,45].



where S_{Au} (S_{vo}) is an adsorption site on the Au (V_2O_5), and e_{vo^-} is an electron from V_2O_5 .

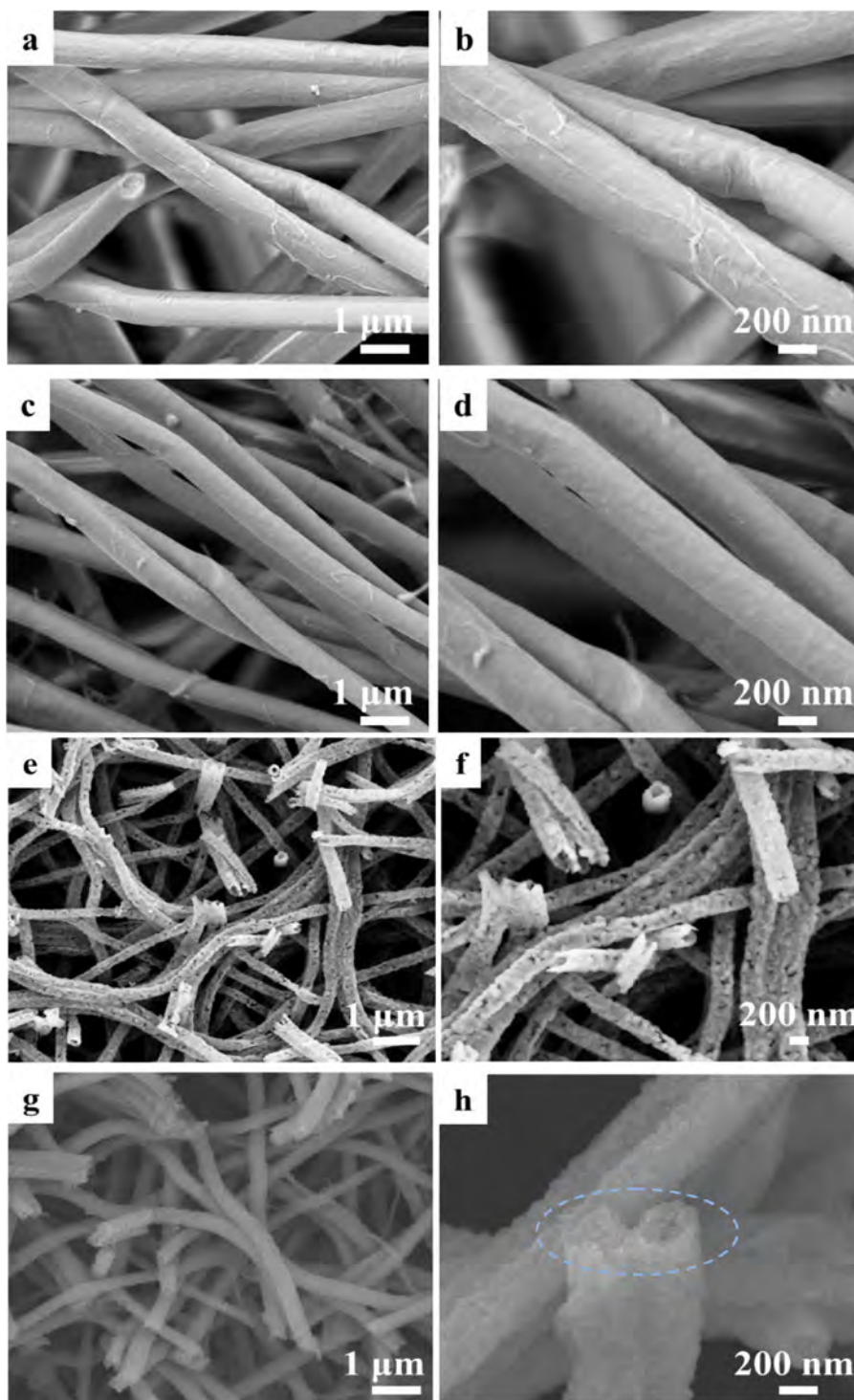


Fig. 4. SEM images of the precursors and the corresponding products after the calcination. (a and b) and (e and f) are PVP/PS/VO(acac)₂ precursor nanofiber and hollow tubular V₂O₅ nanostructures, respectively. (c and d) and (g and h) are PVP/PS/VO(acac)₂/HAuCl₄ precursor nanofiber and hollow tubular Au/V₂O₅ nanostructures, respectively.

Meanwhile, relatively low porosity compared with bare V₂O₅ nanotubes makes the superiority of Au a little eclipsed, which means that more energy is needed to accelerate diffusion, resulting in slight increase in optimal operating temperature. Both sensors show very fast response times, and it seems that the doping of Au nanoparticles has no significant effect toward ethanol gas, even a bit lengthened. This phenomenon is probably attributed to two factors: the improved gas diffusion and mass transport induced by

the higher porosity structure of bare V₂O₅ nanotubes and enhanced surface reaction catalyzed by Au nanoparticles [46].

We also quantitatively compared our results [30,32,47–49] on ethanol sensing performances with those reported by researchers on *n*-type V₂O₅ based ethanol sensors. As shown in Table 1, it is clearly indicated that our hollow V₂O₅ and Au/V₂O₅ electrospun nanotubes exhibit the fastest response/recovery times and top sensing response among those *n*-type V₂O₅ based ethanol sensors.

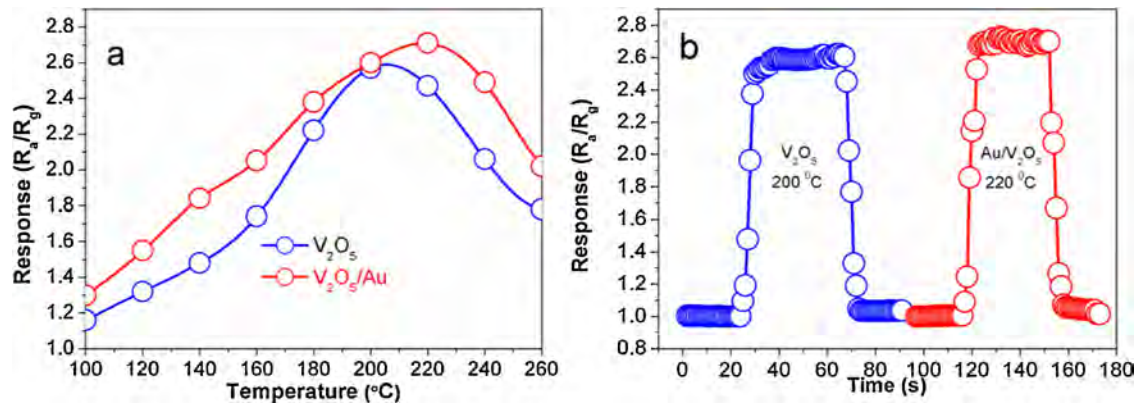


Fig. 5. (a) Responses of V_2O_5 and Au/V_2O_5 nanotubes against 100 ppm ethanol as a function of operating temperature, (b) response/recovery behaviors of V_2O_5 and Au/V_2O_5 nanotubes against 100 ppm ethanol.

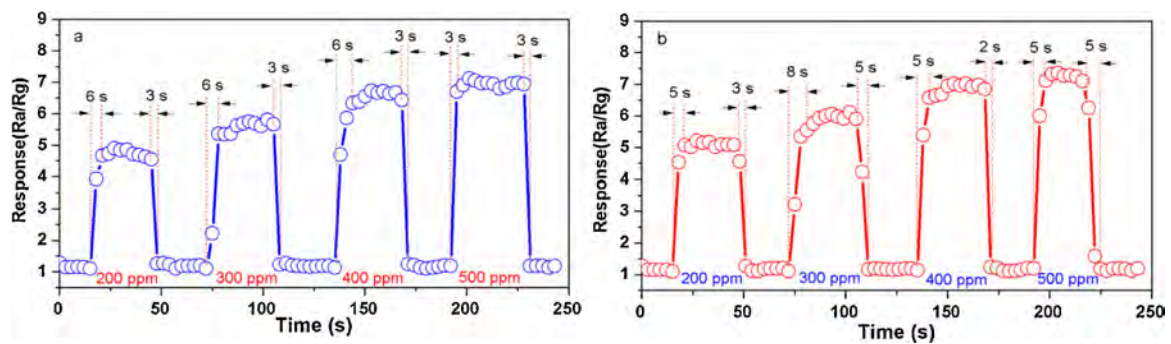


Fig. 6. The dynamic ethanol sensing transients of (a) V_2O_5 and (b) Au/V_2O_5 nanotubes two sensors at different concentrations, ranging from 200 to 500 ppm, at their optimal operating temperature respectively.

We believe that such rapid response/recovery behaviors and good sensing response based on hollow V_2O_5 and Au/V_2O_5 electrospun nanotubes attributed to their unique structures. It has been generally accepted that 1D structure of the samples can improve electric signals to transverse the barriers caused by the target (ethanol) molecules and the ionosorbed oxygen species [50–55]. Additionally, the sensing layers of the nanotubes is

thinner than those of solidified nanofiber, making the wall of the nanotubes can be easily and rapidly penetrated by target (ethanol) molecules and the ionosorbed oxygen species. Thus, the equilibrium between the diffusion rates of the reactants and their surface reaction has been improved [56,57]. Those two main advantages lead to significant gain in the sensing response and rapid response/recovery behaviors of the two hollow V_2O_5 nanotubes.

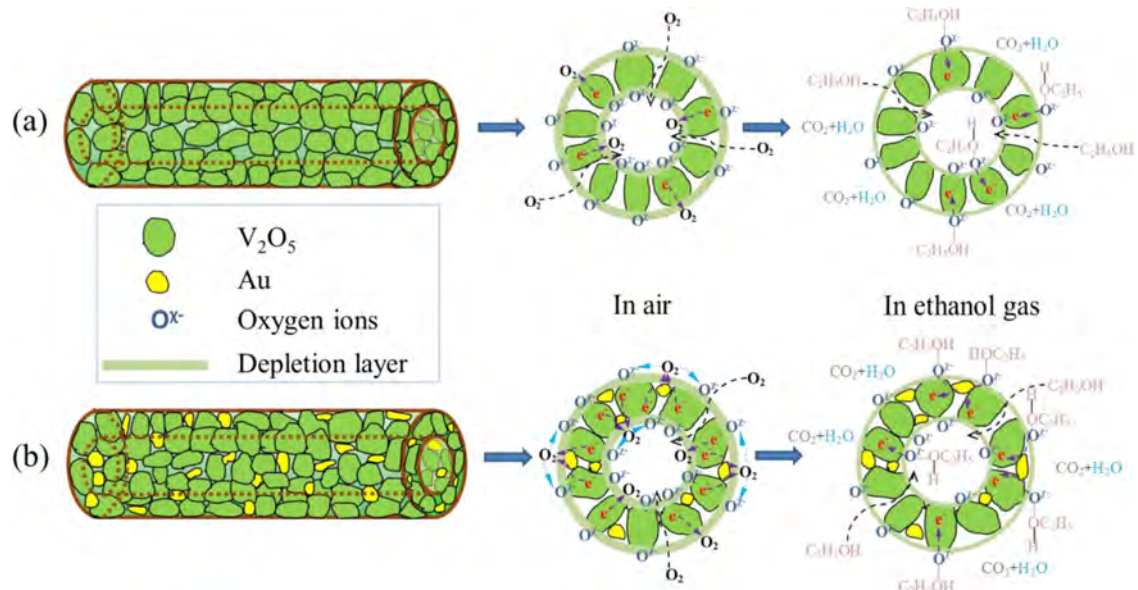


Fig. 7. The Morphologies and sensing mechanism of (a) bare V_2O_5 nanotubes and (b) Au/V_2O_5 nanotubes.

Table 1
Comparison of different *n*-type V₂O₅ nanostructures based ethanol sensors.^a

Materials	Ethanol (ppm)	Operating temperature (°C)	Ra/Rg	Response time/recovery time (s)	Ref.
V ₂ O ₅ tube	100	200	~2.6	5/5	This work
V ₂ O ₅ /Au tube	100	220	~2.7	7/5	
V ₂ O ₅ nanobelts	100	250	~1.7	32/30	[42]
V ₂ O ₅ /TiO ₂ nanobelts	100	250	~2.0	49/85	[42]
V ₂ O ₅ /Fe ₂ O ₃ nanobelts	100	290	~2.3	36/64	[42]
V ₂ O ₅ /SnO ₂ nanobelts	100	290	~3.1	37/126	[42]
V ₂ O ₅ film	300	280~300	~2	–	[43]
Porous V ₂ O ₅ hierarchical	250	250	~5.3	–	[30]
V ₂ O ₅ nanorods formed hollow spheres	100	–	~1.02	23/25	[32]
V ₂ O ₅ /Fe ₂ O ₃ nanotubes	100	270	~1.3	15/20	[44]

^a To give convective comparative data, we have made a suitable transformation to these data by defining S: Ra/Rg.

4. Conclusions

In summary, hollow V₂O₅ and Au/V₂O₅ electrospun nanotubes have been successfully synthesized by combining emulsion electrospinning and post calcination treatment. The as-prepared samples exhibited rapid response/recovery times and good sensing response against ethanol. The present results demonstrated that hollow metal oxide nanostructures fabricated by emulsion electrospinning are very promising in constructing highly efficient gas sensors.

Acknowledgements

This work was supported in part by National Natural Science of China (Nos. 51202302 and 51277185), Chongqing Graduate Student Research Innovation Project (No. CYS14011) and Postdoctoral Science Funded Project of Chongqing (No. Xm201301).

References

- [1] P.G. Collins, K. Bradley, M. Ishigami, A. Zettl, *Science* 287 (2000) 1801.
- [2] J. Kong, N.R. Franklin, C.W. Zhou, M.G. Chapline, S. Peng, K.J. Cho, *Science* 287 (2000) 622.
- [3] F. Favier, E.C. Walter, M.P. Zach, T. Benter, R.M. Penner, *Science* 293 (2001) 2227.
- [4] J. Chen, L.N. Xu, W.Y. Li, X.L. Gou, *Adv. Mater.* 17 (2005) 582.
- [5] F. Schedin, A.K. Geim, S.V. Morozov, E.W. Hill, P. Blake, M.I. Katsnelson, *Nat. Mater.* 6 (2007) 652.
- [6] N. Barsan, U. Weimar, *J. Electroceram.* 7 (2001) 143.
- [7] E. Comini, G. Faglia, G. Sberveglieri, Z.W. Pan, Z.L. Wang, *Appl. Phys. Lett.* 81 (2002) 1869.
- [8] Q. Wan, Q.H. Li, Y.J. Chen, T.H. Wang, X.L. He, J.P. Li, *Appl. Phys. Lett.* 84 (2004) 3654.
- [9] A. Kolmakov, D.O. Klenov, Y. Lilach, S. Stemmer, M. Moskovits, *Nano Lett.* 5 (2005) 667.
- [10] N. Yamazoe, G. Sakai, K. Shimano, *Catal. Surv. Asia* 7 (2003) 63.
- [11] A. Cabot, A. Dieguez, A. Romano-Rodriguez, J.R. Morante, N. Barsan, *Sens. Actuators B* 79 (2001) 98.
- [12] J. Tamaki, *Sens. Lett.* 3 (2005) 89.
- [13] E. Comini, *Anal. Chim. Acta* 568 (2006) 28.
- [14] V.V. Sysoev, B.K. Button, K. Wepsiec, S. Dmitriev, A. Kolmakov, *Nano Lett.* 6 (2006) 1584.
- [15] H.C. Chiu, C.S. Yeh, *J. Phys. Chem. C* 111 (2007) 7256.
- [16] J. Wollenstein, M. Scheulin, N. Herres, W.J. Becker, H. Bottner, *Sens. Mater.* 15 (2003) 239.
- [17] K. Takahashi, S.J. Limmer, Y. Wang, G.Z. Cao, *J. Phys. Chem. B* 108 (2004) 9795.
- [18] A.M. Cao, J.S. Hu, H.P. Liang, L.J. Wan, *Angew. Chem. Int. Ed.* 44 (2005) 4391.
- [19] I. Raible, M. Burghard, U. Schlecht, A. Yasuda, T. Vossmeier, *Sens. Actuators B* 106 (2005) 730.
- [20] J. Liu, H. Xia, D.F. Xue, L. Lu, *Am. Chem. Soc.* 131 (2009) 12086.
- [21] B. Yan, L. Liao, Y.M. You, X.J. Xu, Z. Zheng, Z.X. Shen, *Adv. Mater.* 21 (2009) 2436.
- [22] A.D. Raj, T. Pazhanivel, P.S. Kumar, D. Mangalaraj, D. Nataraj, N. Ponpandian, *Curr. Appl. Phys.* 10 (2010) 531.
- [23] T.Y. Zhai, H.M. Liu, H.Q. Li, X.S. Fang, M.Y. Liao, L. Li, *Adv. Mater.* 22 (2010) 2547.
- [24] N. Izu, G. Hagen, D. Schonauer, U. Roder-Roith, R. Moos, *Sensors* 11 (2011) 2982.
- [25] W. Jin, W. Chen, Y. Lu, C.X. Zhao, Y. Dai, *Nanosci. Nanotech.* 11 (2011) 10834.
- [26] J.A. Yan, A. Sumbaja, E. Khoo, P.S. Lee, *Adv. Mater.* 23 (2011) 746.
- [27] V. Modafferi, G. Panzera, A. Donato, P.L. Antonucci, C. Cannilla, N. Donato, *Sens. Actuators B* 163 (2012) 61.
- [28] A.D. Raj, P.S. Kumar, Q. Yang, D. Mangalaraj, *Physica E* 44 (2012) 1490.
- [29] H.H. Yin, K. Yu, H. Peng, Z.L. Zhang, R. Huang, J. Travas-Sejdic, *Mater. Chem.* 22 (2012) 5013.
- [30] Y. Qin, G. Fan, K. Liu, M. Hu, *Sens. Actuators B* 190 (2014) 141.
- [31] J.F. Liu, X. Wang, Q. Peng, Y.D. Li, *Adv. Mater.* 17 (2005) 764.
- [32] A. Dhayal Raj, T. Pazhanivel, P. Suresh Kumar, D. Mangalaraj, D. Nataraj, N. Ponpandian, *Curr. Appl. Phys.* 10 (2010) 531.
- [33] V. Modafferi, G. Panzera, A. Donato, P.L. Antonucci, C. Cannilla, N. Donato, *Sens. Actuators B* 163 (2012) 61.
- [34] W. Jin, B.T. Dong, W. Chen, C.X. Zhao, L.Q. Mai, Y. Dai, *Sens. Actuators B* 145 (2010) 211.
- [35] Z.Y. Li, X.G. Wang, T. Lin, *Mater. Chem. A* 2 (2014) 13655.
- [36] T. Lin, H. Wang, H. Wang, X. Wang, *Nanotechnology* 15 (2004) 1375.
- [37] P. Feng, X.Y. Xue, Y.G. Liu, T.H. Wang, *Appl. Phys. Lett.* 89 (2006) 32.
- [38] Y.X. Liang, Y.J. Chen, J.H. Wang, *Appl. Phys. Lett.* 85 (2004) 666.
- [39] X. Xu, X. Zhuang, X. Chen, X. Wang, L. Yang, X. Jing, *Macromol. Rapid Commun.* 27 (2006) 1637.
- [40] A.V. Bazilevsky, A.L. Yarin, C.M. Megaridis, *Langmuir* 23 (2007) 2311.
- [41] C. Kim, Y.I. Jeong, B.T.N. Ngoc, K.S. Yang, M. Kojima, Y.A. Kim, *Small* 3 (2007) 91.
- [42] H. Chen, J. Di, N. Wang, H. Dong, J. Wu, Y. Zhao, *Small* 7 (2011) 1779.
- [43] X.Z. Wang, S. Qiu, C.Z. He, G.X. Lu, W. Liu, J.R. Liu, *RSC Adv.* 3 (2013) 19002.
- [44] L.W. Wang, S.R. Wang, M.J. Xun, X.J. Hu, *Phys. Chem. Chem. Phys.* 15 (2013) 17179.
- [45] P. Montment, J.C. Marchand, R. Lalauze, *Sens. Actuators B* 95 (2003) 83.
- [46] J. Zhang, X.H. Liu, S.H. Wu, M.J. Xu, *Mater. Chem.* 20 (2010) 6453.
- [47] J. Liu, X. Wang, Q. Peng, Y. Li, *Sens. Actuators B* 115 (2006) 481.
- [48] R. Rella, P. Siciliano, A. Cricenti, R. Generosi, M. Girasole, L. Vanzetti, *Thin Solid Films* 349 (1999) 254.
- [49] W. Jin, B. Dong, W. Chen, C. Zhao, L. Mai, Y. Dai, *Sens. Actuators B* 145 (2010) 211.
- [50] A. Kolmakov, M. Moskovits, *Annu. Rev. Mater. Res.* 34 (2004) 151.
- [51] Z.Y. Li, H.N. Zhang, W. Zheng, W. Wang, H.M. Huang, C. Wang, *J. Am. Chem. Soc.* 130 (2008) 5036.
- [52] H.N. Zhang, Z.Y. Li, L. Liu, C. Wang, Y. Wei, *Talanta* 79 (2009) 953.
- [53] W. Zheng, X.F. Lu, W. Wang, Z.Y. Li, H.N. Zhang, Y. Wang, *Sens. Actuators B* 142 (2009) 61.
- [54] Z.J. Wang, Z.Y. Li, J.H. Sun, H.N. Zhang, W. Wang, W. Zheng, *Phys. Chem. C* 114 (2010) 6100.
- [55] Z.J. Wang, Z.Y. Li, T.T. Jiang, X.R. Xu, C. Wang, *ACS Appl. Mater. Int.* 5 (2013) 2013–2021.
- [56] T. Hyodo, K. Sasahara, Y. Shimizu, M. Egashira, *Sens. Actuators B* 106 (2005) 580.
- [57] Z.P. Li, Q.Q. Zhao, W.L. Fan, J.H. Zhan, *Nanoscale* 3 (2011) 1646.